Chemotherapeutic molecular switch behavior of aryl-substituted tetracarboxylic dianhydrides

Hamdullah Khadim Sheikh^{1,2}*, Tanzila Arshad¹, Haroon Khan^{3,4}, Uzma Habib⁵, Jamelah Saleh Al-Otaibi⁶, Tan Ching Siang⁷, Faiza Iqbal⁸ and Umbreen Farrukh⁹

¹Department of Pharmacognosy, Faculty of Pharmacy & Pharmaceutical Sciences, University of Karachi, Pakistan

Abstract: In this study, we synthesized aryl-substituted tetracarboxylic acid dianhydride (TCDA) diastereomers having potential for chemoselective DNA alkylation. The TCDAs were obtained through a radical-initiated addition chain reaction. Diastereomeric reaction mixture was characterized by FTIR, UV, EI-MS, and elemental analysis. Quantum Mechanical (QM) calculations, including relaxed potential energy surface (PES) scans at B3LYP/6311+G (d,p) and MP2/6-31G optimizations of global minima of each diastereomer, revealed that the most stable and polar aryl-substituted TCDA diastereomers adopt non-anti dihedral geometries between the two anhydride rings. This conformation effectively reduces nucleophilic accessibility on the C=O, thereby limiting nucleophilic attack under physiological conditions, with possible activation under mildly acidic microenvironments of tumors. The stability and polarity are additional helpful drug attributes. Further validation of reduced reactivity came from biological screening of the aryl-substituted diastereomeric mixture against human HeLa cancer cell line, which demonstrated reduced reactivity compared to alkyl TCDA control analogs, despite both sharing the same crosslinking TCDA arm. These computational and bioactivity results suggest that aryl substitution imposes conformational constraints that induce environment-dependent differences in reactivity. Overall, this study shows that stereoelectronic factors can modulate reactivity, offering a rationale for the development of selective therapeutic agents. Further investigations are underway to evaluate the individual bioactivities of isolated diastereomers.

Keywords: Acylation; Antineoplastic agents; Deoxyribonucleic acids; Organic synthesis; Quantum mechanics

Submitted on 13-09-2024 - Revised on 20-07-2025 - Accepted on 22-07-2025

INTRODUCTION

Alkylating agents are used in anticancer chemotherapy due to their ability to disrupt deoxyribonucleic acid (DNA) integrity through covalent bonding modifications. Their therapeutic character stems from their electrophilic sites, which enable reaction with nucleobases of DNA strands. Classical alkylating agents such as N-mustards, nitrosoureas, aziridines and Pt-complexes have demonstrated efficacy through such mechanisms, but suffer from off-target toxicity and poor chemoselectivity due to uncontrolled reactivity (Karati *et al.*, 2022; Sheikh *et al.*, 2024).

To address these limitations, recent strategies have focused on structural and electronic modulation of alkylating agents to achieve environment-dependent reactivity (Sheikh *et al.*, 2018). The tumor microenvironment, being mildly acidic in comparison to

healthy cells, provides an opportunity for selective activation of pH-responsive agents (Cao et al., 2015; Hulikova et al., 2013). Hence, we propose the use of conformationally controlled molecular switches as DNA crosslinking acylating agents with improved selectivity. TCDAs possess dual electrophilic sites capable of acylation (Fig. 1), but their reactivity can be modulated through steric and electronic constraints. This study investigates aryl-substituted TCDA derivatives with controlled conformation to reduce reactivity while enabling environment-dependent modulation, such as the mildly acidic conditions of tumor microenvironments. The design rationale is based on molecular switch behavior, referring to a conformation induced suppression of reactivity of the designed alkylating agent under neutral pH, which may need acidic catalytic conditions for reaction. The aryl substitution distorts the antidihedral angle between the two TCDA cores, thereby shielding the C=O groups. This masking of electrophilicity under physiological pH and possible

*Corresponding author: e-mail: hamdullah.khadim.sheikh@gmail.com

²BioLab, Instituto Universitario de Bio-Orgánica Antonio González (IUBO-AG), Universidad de La Laguna, Spain

³Department of Pharmacy, Abdul Wali Khan University Mardan, Pakistan

⁴Department of Pharmacy, Korea University, Sejong, South Korea

School of Interdisciplinary Engineering and Sciences (SINES), National University of Sciences and Technology (NUST), Pakistan

⁶Department of Chemistry, College of Science, Princess Nourah Bint Abdulrahman University, Saudi Arabia

⁷School of Pharmacy, KPJ Healthcare University, Nilai, Malaysia

⁸University of Health Sciences, Lahore, Pakistan

⁹Department of Pharmacognosy, Faculty of Pharmacy and Pharmaceutical Sciences, University of Karachi, Dow College of Pharmacy, Dow University of Health Sciences, Pakistan

reactivation under mildly acidic conditions has been proposed as switch-like behavior.

The aryl substitution on the TCDA backbone controls the dihedral angle between the two anhydride rings that directly influences C=O orbital exposure and, thus, the electrophilic potential. Specifically, the dihedral angle (θ_a) determines the accessibility of lowest unoccupied molecular orbitals (LUMO) of the C=O, with the anti conformation ($\theta=180^\circ$) being most permissive to nucleophilic attack due to minimal steric shielding (fig. 2). However, aryl substitution at the TCDA core disrupts this anti geometry, favoring a folded conformation that shields the C=O and limits reactivity under neutral conditions (fig. 1 and 2). This conformational effect may act as an intrinsic control of electrophilicity, forming the basis for molecular switch behavior.

Based on these structural considerations, the present work aims to investigate the hypothesis that aryl substitution stereoelectronic constraints capable controlling electrophilicity or inducing molecular switch behaviour in presence of environmental acidity, an effect consistent with the mildly acidic fumor microenvironment. These findings will reinforce the concept of dihedral geometry as a design feature in conformationally controlled molecular switches for selective anticancer therapy.

MATERIALS AND METHODS

Solvents and reagents used in synthesis, were of analytical grade. The mass spectra were recorded on MAT 312 and MAT 113D mass spectrometers (Varian, USA). The IR spectra were recorded on a Bruker Optics ATR-Alpha spectrophotometer (Germany). UV spectra were taken on Thermoscientific evolution-300 UV-V spectrophotometer. Reaction progress was evaluated on thin-layer chromatography (TLC) using Merck pre-coated silica gel $60~F_{254}~20~\times~20~$ cm aluminum sheets. Spots were observed under UV light at 254 and 366 nm. The entire dataset of QM calculations performed in this study and the supplementary information are available at https://dx.doi.org/10.17632/ypjfdst7nh.1

Synthesis of TCDA (6) and (6')

Maleic anhydride (3.15 mmol) is added to ethylbenzene (3) (3.99 mmol) in an inert environment of N₂. This reaction mixture is refluxed at 145-155 °C. At the same time, ethylbenzene (2.22 mmol) containing azobisisobutyronitrile (0.03653 mmol) is added in a dropwise manner (0.002 mol/min). The remaining maleic anhydride is also added (0.0023 mol/min). Additional heating up to 160-170 °C is provided for the next 17-18 minutes. At the end of this period, colorless crystals of TCDA are formed, which are filtered and transferred to a distillation flask. Unreacted ethyl benzene is vacuum

distilled. The residue containing TCDA diastereomers is further dried, washed with cold n-hexane, and recrystallized from hot acetone to afford a diastereomeric mixture of TCDA (6). Same steps were used for TCDA (6'), replacing ethylbenzene with liquefied butane (3') as the alkyl donor. The granules had a melting point of approximately 152 °C. The same methodology is used to synthesize (6') with liquefied butane (3'). The details concerning the observed physical properties and spectroscopic molecular structure elucidation are given in results section. while spectra are given in sections A (FTIR, fig. S1), B (UV, fig. S2), and C (MS, fig. S3) of the supplementary information (SI).

Comparative anticancer assay

Reaction mixtures of TCDA (6) and TCDA (6'), each comprising their respective diastereomeric mixture, were evaluated for antiproliferative activity using the HeLa human cervical cancer cell line. Cells were cultured in Dulbecco's Modified Eagle Medium (DMEM) supplemented with 10% fetal bovine serum (FBS) and 1% penicillin-streptomycin and maintained at 37 °C in a humidified 5% CO₂ incubator. Compounds were dissolved in DMSO (final concentration <0.5%) and added to cells seeded at a density of 5×10^3 cells/well in 96-well plates. After 48 hours of incubation under physiological pH (7.4), cell survival was assessed using the MTT assay (Ghasemi et al., 2021). Absorbance was recorded at 570 nm, and relative viability was calculated with respect to untreated controls (Benov, 2021). TCDA (6) exhibited reduced cytotoxicity compared to the butane-derived TCDA (6'), despite both sharing the same reactive core, consistent with conformational shielding of electrophilic centers in the aryl-substituted structure (Table 1).

QM relaxed potential energy scan

Quantum mechanical (QM) calculations were performed using Gaussian 16 software (Sheikh et al., 2022; Malyshkina et al., 2021) to explore the dihedral angle, relative stability and polar character (dipole moment) of the sixteen possible diastereomers of the synthesized arylsubstituted TCDAs (6a-6p). Initially, each diastereomer was geometry optimized at the Hartree-Fock (HF)/6-311G level to generate starting structures. The output geometries were then re-optimized using density functional theory (DFT) at the B3LYP/6-311G level to incorporate electron correlation to improve accuracy. To locate the global minimum for each diastereomer, relaxed potential energy surface (PES) scans were conducted along the central dihedral axis (O=C-C-C-C=O) at the B3LYP/6-311+G(d,p) levels (Paulraj et al., 2013). The lowest-energy conformers from these scans were further refined using second-order Møller-Plesset perturbation theory (MP2) at the MP2/3-21G level. Finally, singlepoint energy calculations were carried out at the MP2/6-31G level to obtain accurate relative electronic energies

for comparison (Loipersberger *et al.*, 2021). All structures were fully optimized (max RMS gradient $< 1 \times 10^{-5}$, indicating convergence).

Dihedral angles (θ_a) between the two anhydride planes were extracted from the optimized geometries and are reported using the standard -180° to +180° convention, where negative values indicate counterclockwise torsion (Table 2). Electronic energies (a.u) of individual diastereomers and relative energies (in kcal/mol) were computed for each diastereomer with respect to the global minima of most stable diastereomer (6d). Dipole moments were noted for insights onto electronic asymmetry, which affects solvation and reactivity. Dipole moment and energy values were used to rank diastereomers for their folded or extended conformational bias and reactivity profiles. Complete QM input files, output logs, and checkpoint (.chk) files for all diastereomers (6a-6p) are provided in the dataset. Folder names reflect the model chemistry used at each step.

RESULTS

The crosslinking acylation of TCDA (6) with guanine is shown in fig. 1, while the synthesis scheme of TCDA (6) and TCDA (6') is presented in fig. 2. Spectroscopic data are provided in Section A (FTIR, fig. S1), Section B (UV–Vis, fig. S2), and Section C (EI–MS, fig. S3) of the supplementary information. Relaxed potential energy Surface scans (PESS) of diastereomers (6a-6p) are provided in Section D (fig. S5-S20) while their dihedral angles (θ_a) are provided in Section E (Fig. S21-S36) of Supplementary information. Activity against HeLa cells is summarized in Table 1, while Table 2 lists the QM-calculated dihedral angle (θ_a), electronic energy, dipole moment, and relative energies for the sixteen TCDA (6a–6p) diastereomers.

1-(1-phenylethyl)tetrahydro-[3,3'-bifuran]-2,2',5,5'-tetraone (6)

Colorless needle-like crystalline solid, Soluble in DMSO, DMF, CHCl₃; Yield: 54% on Ethylbenzene.; TLC (Si gel, Ethyl Acetate/Hexane 3:1): $R_f=0.42$, Single major spot under UV (254 nm).; Mp: 152 °C.; Anal. Calculated for $C_{16}H_{14}O_6$: C, 63.57; H, 4.67; O, 31.76% Found: C, 63.55; H, 4.75; O, 31.80%.; FT-IR (KBr, ν_m ax, cm⁻¹): 1886, 1767 (C=O, asym. and sym. stretch of anhydride), 1634, 1585 (C=C aromatic), 1218, 1260 (C-O-C anhydride), 3057 (C-H aromatic), 2874 (C-H aliphatic).; UV-Vis (CHCl₃, λ_m ax): 258.00 nm (A = 3.073, ϵ = 7682.5 L·mol⁻¹·cm⁻¹).; EI-MS (m/z): 302.079 [M]⁺, consistent with the molecular formula $C_{16}H_{14}O_6$.

4-(sec-butyl)tetrahydro-[3,3'-bifuran]-2,2',5,5'-tetraone (6')

Colorless crystalline solid, Soluble in DMSO, DMF, CHCl₃; Yield: 40% on Butane.; Mp: 90°C.; Anal.

Calculated for $C_{12}H_{14}O_6$: C, 56.69; H, 5.55; O, 37.76%. Found: C, 56.66; H, 5.558; O, 37.79%.; FT-IR (KBr, v_max, cm⁻¹): 1886, 1767 (C=O, asym. and sym. stretch of anhydride), 1218, 1261 (C-O-C anhydride), 2873 (C-H aliphatic).; UV-Vis (CHCl₃, λ _max): 253.00 nm (A = 0.067, ϵ = 167.5 L·mol⁻¹·cm⁻¹).; EI-MS (m/z): 254.079 [M], consistent with the molecular formula $C_{12}H_{14}O_6$.

DISCUSSION

Synthesis

The synthesis of the aryl-substituted TCDA (6) proceeded via a radical-initiated process under N2 environment, using AIBN as a thermally activated radical generator. The reaction produced a complex mixture of (sixteen possible) diastereomers, due to the presence of four stereogenic centers on the TCDA arm (Fig. 2). In the arylsubstituted derivatives, radical attack preferentially occurred at the benzylic carbon of ethylbenzene due to resonance stabilization of the intermediate radical species. This stabilization reduces the activation energy barrier, directing chain propagation selectively through the aryl methylene position. In the alkyl-substituted (butanebased) system, the radical attack favored the more stable 2º carbon, driven by inductive and hyperconjugative stabilization rather than resonance (fig. 2). Both systems terminated predominantly at the n = 2 stage, forming tetracarboxylic dianhydrides rather than extended oligomers, likely due to intramolecular anhydride ring closure, which effectively quenches radical propagation sequestering the reactive termini into conformationally stable cyclic structure. Synthesized product mixture (6) gave M⁺ at 302.0 m/z in EI-MS. The other TCDA (6') gave M.+ at 254.0 m/z (See section C of Supplementary Information; fig. S3-S4).

QM relaxed potential energy scan

To confirm non-anti dihedral angle between the two anhydride rings in diastereomers of molecule (6), a series of hierarchical QM calculations was performed. Initial geometry optimizations at HF/6-311G served as input for B3LYP/6-311G and then B3LYP/6-311+G(d,p)optimizations. This incorporated electron correlation with improved polarization and diffuse function treatment for addressing electronic effects in flexible polycyclic systems. Relaxed potential energy surface (PES) scans were then performed along the central O=C-C-C-C=O dihedral axis for all diastereomers at B3LYP/6-311G levels (6a-6p) (See fig. S5-S20 of Section Dof Supplementary Information) (Paulraj et al., 2013). The structure corresponding to global minimum were further refined at MP2/3-21G level. Final single-point energy calculations at MP2/6-31G provided accurate relative stabilities. The dihedral angle (θ_a) between the two anhydride planes deviated significantly from the anticonfiguration (180°) in the majority of cases, adopting lower-energy folded geometries (See fig. S21-S36 of Section E of Supplementary information).

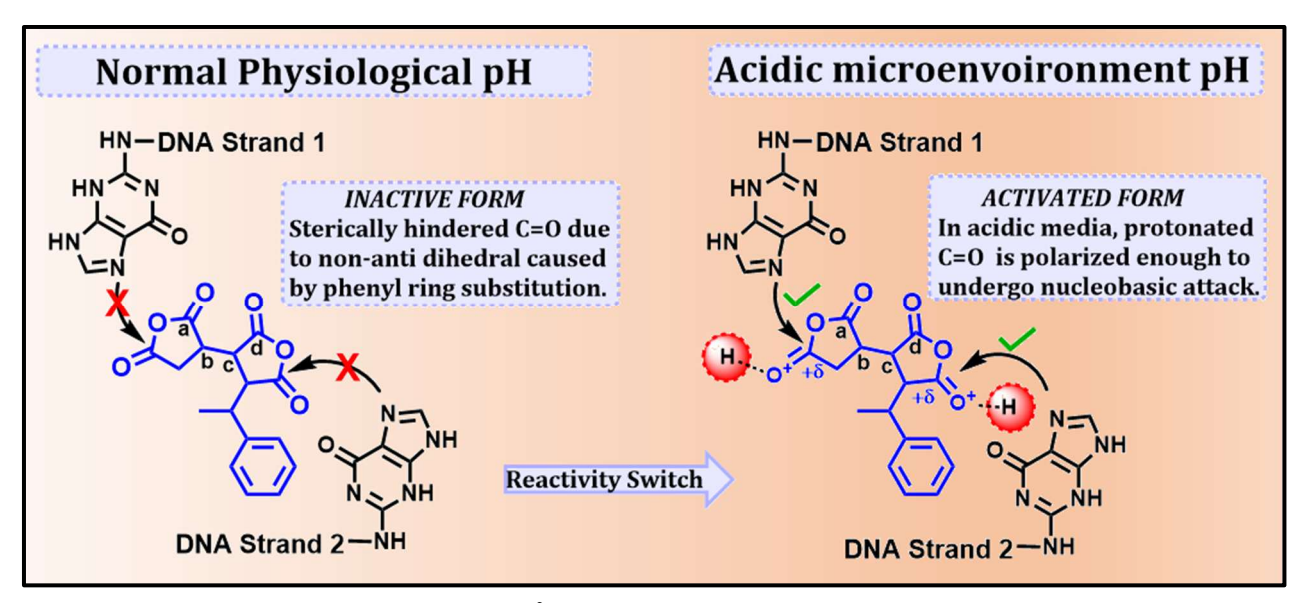


Fig. 1: Proposed crosslinking acylation of sp^2 hybridized N atom of imidazole ring of Guanine nucleobase at dianhydride rings of TCDA (6). Dihedral angle (θ_a) along O=C(a)-C(b)-C(c)-C(d)=O is also shown.

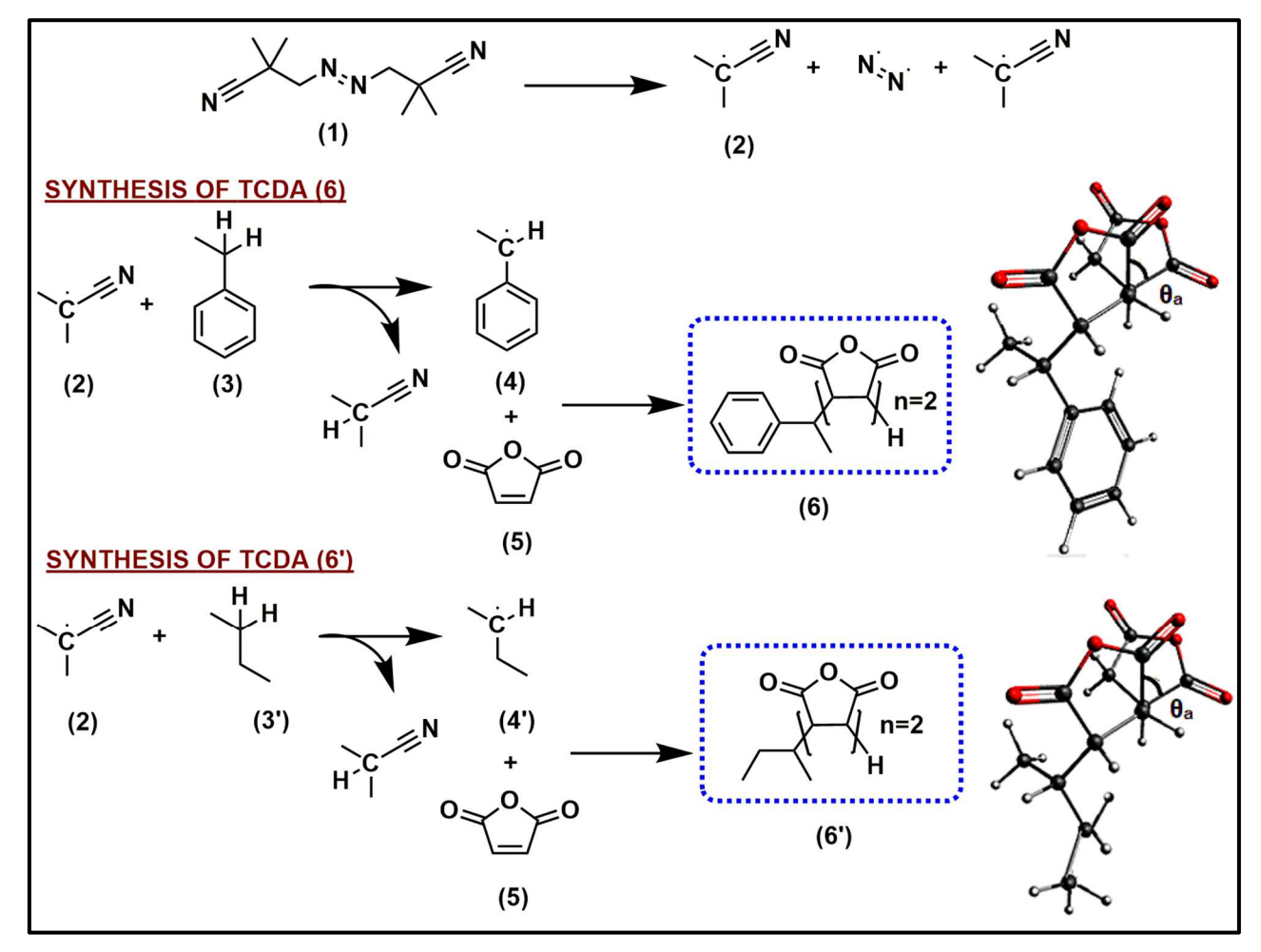


Fig. 2: Synthesis scheme of TCDA (6) and (6'). Benzylic (4) and 2^0 alkyl (4') radicals are shown. Dihedral angle (θ_a) between two anhydride rings is also shown.

Table 1: Antiproliferative activity of TCDA (6) and (6') against HeLa cells at pH 7.4 (48 h exposure), performed at 50 μ M in three replicates, each in triplicate (n = 9). The % inhibition was calculated relative to the DMSO as control.

| Compound | Concentration (µM) | Cell viability (%) ± SD | % Inhibition | Interpretation |
|----------------|--------------------|-------------------------|--------------|-------------------|
| TCDA (6) | 50 | 68.3 ± 2.5 | 31.7 | Lower inhibition |
| TCDA (6') | 50 | 41.6 ± 1.8 | 58.4 | Higher inhibition |
| DMSO (Solvent) | _ | 100.0 ± 1.1 | 0.0 | No inhibition |

Table 2: Summary of QM calculation results for sixteen diastereomer of TCDA (6a-6p): Stereochemical configuration, optimized dihedral angle (θ_a), electronic energy (Hartrees), dipole moment (D), relative energy (kcal/mol), and relative dipole moment ($\Delta\mu$) compared to the most stable conformer (6d).

| D: | C | D:1 11 | | Dipole | Relative | Relative Dipole |
|---------------------|-----------------------|-----------------------------|----------------|---------|------------|-----------------|
| Diastereomer No. | Configuration of TCDA | Dihedral angle (θ_a) | Energy (a.u.) | Moment | Energy | Moment |
| | | | | (Debye) | (kcal/mol) | (Debye) |
| 6a | R,R,R,R | 173.43 | -1064.95337098 | 2.0590 | 3.072918 | -8.3007 |
| 6b | S,S,S,S | -173.43 | -1064.95337098 | 2.0590 | 3.072918 | -8.3007 |
| 6c | R,R,R,S | -176.10 | -1064.95297019 | 2.2761 | 3.324417 | -8.0836 |
| 6d | S,S,S,R | -55.09 | -1064.95826799 | 10.3597 | 0 | 0 |
| 6e | R,S,S,S | -72.48 | -1064.95595660 | 9.0667 | 1.450418 | -1.2930 |
| 6f | S,R,R,R | 72.48 | -1064.95595660 | 9.0667 | 1.450418 | -1.2930 |
| 6g | R,R,S,S | -176.66 | -1064.95237952 | 1.9647 | 3.695068 | -8.3950 |
| 6h | S,S,R,R | 176.66 | -1064.95237952 | 1.9647 | 3.695068 | -8.3950 |
| 6i | R,S,R,R | 163.60 | -1064.94838853 | 3.2359 | 6.19945 | -7.1238 |
| 6 <u>j</u> | S,R,S,S | -73.33 | -1064.94538946 | 9.5908 | 8.081393 | -0.7689 |
| 6k | R,S,S,R | 47.42 | -1064.95754669 | 10.3867 | 0.452622 | 0.0270 |
| 61 | S,R,R,S | -48.21 | -1064.95136555 | 9.8745 | 4.331343 | -0.4852 |
| 6m | R,R,S,R | 53.41 | -1064.95438783 | 11.0312 | 2.434835 | 0.6715 |
| 6n | S,S,R,S | -38.12 | -1064.94652958 | 8.6168 | 7.365958 | -1.7429 |
| 60 | R,S,R,S | -33.92 | -1064.94456504 | 8.4341 | 8.598724 | -1.9256 |
| 6p | S,R,S,R | 51.13 | -1064.94652958 | 8.6168 | 7.365958 | -1.7429 |

These non-anti conformations in the MP2-optimized global minima limited the exposure of LUMO orbitals on the C=O, making them less accessible for nucleophilic attack under neutral or physiological pH. Thus, reactivity control is imposed by steric restriction on the dihedral angle (θ_a) imposed by aryl substitution. Among the sixteen possible diastereomers (2⁴= 16), diastereomer 6d (S,S,S,R) was identified as the most stable with an energy of -1064.95827 a.u. and the highest dipole moment (10.36 D). The majority adopted non-anti dihedral geometries in their MP2-optimized global minima, showing a conformational bias toward folded states caused by the aryl ring substitution. Diastereomers 6d (S,S,S,R), 6l (R,S,S,R), 6e (R,S,S,S), and 6n (R,R,S,R) emerged as the most low-energy conformers and all had non-anti dihedral between the TCDA rings. Diastereomer 6d, with a dihedral angle of -55.09°, was the most stable ($\Delta E = 0.00$ kcal/mol) and exhibited a high dipole moment of 10.36 D (relative dipole $\Delta\mu=0.00$ D). 6l, with $\theta_a=47.42^\circ$, had a relative energy of 0.45 kcal/mol and a dipole of 10.39 D $(\Delta \mu = +0.03 \text{ D})$, while 6e, adopting a geometry of -72.48°, was slightly higher in energy (1.45 kcal/mol) but still maintained a strong dipole moment of 9.07 D ($\Delta \mu = -1.29$

Similarly, 6n, with $\theta_a = 53.41^{\circ}$, displayed both a high dipole of 11.03 D ($\Delta\mu$ = +0.67 D) and a low relative energy of 2.43 kcal/mol. These values categorize these more stable diastereomers as folded thus less exposed C=O in neutral conditions, while being polar (electronic asymmetry) for solvation and interaction with nucleobases. In contrast, diastereomers 6a (R,R,R,R) and 6b (S,S,S,S) had near-anti dihedral ($\theta_a = 173.43^{\circ}$ and -173.43°, respectively) and relatively low in energy ($\Delta E =$ 3.07 kcal/mol each), exhibited significantly lower dipole moments of 2.06 D ($\Delta\mu$ = -8.30 D), suggesting more exposure of C=O for higher reactivity and reduced electrostatic profile for solvation or interaction with biological sites. These diastereomers likely contribute less to the overall switch-like behavior of the mixture. By comparison, diastereomers 6e (R,S,S,S) and 6f (S,R,R,R) adopted near-folded geometries ($\theta_a = 72^{\circ}$), with moderate dipoles (9.07 D) and favorable relative energies (1.45 kcal/mol), indicating reduced C=O exposure under physiological conditions while maintaining strong solvation potential and nucleobase interaction. Together, these results support the hypothesis that non-anti dihedral wielding diastereomers with less exposed C=O were more stable (low ΔE) and were more polar (higher dipole), thus will be less reactive in neutral physiological conditions yet solvated and interactive with DNA nucleobases. These molecules may become more susceptible to nucleophilic acyl substitution under mildly acidic conditions. In the case of the alkyl-substituted compound (6'), the flexible aliphatic backbone allows adoption of conformers with more open or closer to anti-dihedral angles. Consequently, the electrophilic C=O in (6') remained more exposed to nucleophilic attack, unlike the aryl system (6).

Several diastereomeric pairs exhibited identical electronic energy and dipole moment values, reflecting their enantiomeric relationship. These include diastereomers 6a (R,R,R,R) and 6b (S,S,S,S), 6g (R,R,S,S) and 6h (S,S,R,R), as well as 60 (S,S,R,S) and 6p (S,R,S,R). In the absence of a chiral environment, enantiomers have energetically degenerate conformations and show same dipole orientations and magnitudes. These enantiomeric pairs confirm the overall folding trend in the diastereomers, as both mirror forms equally support the reduced-reactivity conformation. In other cases, relaxed PES scans located different low-energy conformers for each enantiomer, so the reported values reflect the lowest minimum found for that stereoisomer rather than a strict mirror of its partner.

Comparative anticancer activity

To validate the effect of hindered electrophilic site on reduced bioactivity, preliminary antiproliferative assays were carried out using the diastereomeric mixtures of (6) and (6') against human HeLa cancer cell line. At a fixed concentration of 50 µM under physiological pH (7.4), TCDA (6) showed a cell viability of $68.3 \pm 2.5\%$, corresponding to 31.7% inhibition, while alkyl-substituted TCDA (6') exhibited $41.6 \pm 1.8\%$ viability at 58.4%inhibition (Table 1). These results were obtained from three independent experiments, each performed in triplicate, with absorbance measured via the MTT assay. The aryl-substituted TCDA (6) demonstrated lower cytotoxicity compared to the alkyl-substituted TCDA (6'), despite both sharing the same reactive TCDA core. This confirms that conformational shielding of the electrophilic C=O orbitals in (6) reduces its alkylating potential under neutral physiological conditions.

While the single-dose data suggest a trend, comprehensive dose response curves and IC₅₀ will be determined in subsequent studies. The difference in cytotoxicity underscores how conformational changes may influence bioactivity and trigger environment-sensitive activation, particularly within mildly acidic tumor microenvironments. In contrast, the alkyl-substituted TCDA (6') showed higher cytotoxicity, implying a lack of conformational control and higher C=O exposure. This finding is consistent with the idea that conformational changes introduced by aryl-

substitution could influence bioactivity in an environment-sensitive manner.

Future implications for chemoselective drug design

These results collectively support the basic hypothesis of this study that steric constraints introduced through substitution can modulate the reactivity of electrophilic functional groups in bioactive ligands. experimentally observed reduced anti-cancer activity and the computationally confirmed non-anti geometry of the aryl-substituted TCDAs (6) together show a viable strategy for designing chemoselective alkylating agents with controlled reactivity. This work thus provides a structural rationale that could be explored in the design of pH-responsive DNA-alkylating agents with potentially improved selectivity (Sheikh et al., 2018). This modulation of ligand structure to control activation aligns with broader strategies used to sensitize cancer cells to specific chemotherapeutics (Huang et al., 2023). Such rational drug design by means of structurally controlled reactivity offers future translational potential in designing prodrugs with even more refined reactivity for tumor environments, allowing for selective activation and reduced toxicity. The primary aim of this study was to perform a structure-reactivity correlation by comparing diastereomeric mixtures of aryl and alkyl substituted TCDAs with same electrophilic pharmacophore. Comparative pH-dependent testing against standard anticancer agents like cisplatin, as well as determination of IC₅₀ values on multiple cancer cell lines, will be pursued in follow-up studies after resolving the individual diastereomers to facilitate full Structure-activity relationship (SAR) analysis.

CONCLUSION

This study demonstrates that aryl-substituted TCDAs are proposed to function as conformationally controlled alkylating agents with potential for selective DNA targeting under mildly acidic conditions. Bioactivity screening against the HeLa cancer cell line showed reduced cytotoxicity for aryl-substituted compared to control alkyl-substituted analogs, despite both sharing the same electrophilic **TCDA** pharmacophore. Ouantum mechanical calculations performed on all sixteen possible diastereomers of the aryl-substituted TCDAs revealed that most stable and polar diastereomers adopt non-anti dihedral geometries due to aryl substitution, leading to reduced exposure of the C=O groups and decreased reactivity under physiological conditions. This supports the hypothesis that aryl substitution imposes stereoelectronic constraints that may contribute to environment-sensitive modulation of reactivity. These results highlight the potential of sterically tuned scaffolds for designing chemoselective therapeutic agents. Future work will focus on isolating individual diastereomers and evaluating and further finetune their selective biological activities.

Acknowledgments

- School of Interdisciplinary Engineering and Sciences (SINES), National University of Sciences and Technology (NUST), Pakistan.
- Coimbra Chemistry Centre (Centro de Química de Coimbra, CQC), University of Coimbra, Portugal.
- Researchers Supporting Project Number (PNURSP2025R13), Princess Nourah Bint Abdulrahman University.

Authors' contributions

Hamdullah Khadim Sheikh and Tanzila Conceptualization; Hamdullah Khadim Sheikh and Haroon Khan: Data curation; Hamdullah Khadim Sheikh: Formal analysis: Hamdullah Khadim Sheikh, Tanzila Arshad, Faiza Iqbal, Umbreen Farrukh, Jamelah Saleh Al-Otaibi and Tan Ching Siang: Investigation; Hamdullah Khadim Sheikh, Tanzila Arshad, Jamelah Saleh Al-Otaibi and Tan Ching Siang: Methodology; Uzma Habib: Resources and Software; Hamdullah Khadim Sheikh: Supervision; Hamdullah Khadim Sheikh and Tanzila Arshad: Validation and Visualization; Uzma Habib: Project administration; Hamdullah Khadim Sheikh and Tanzila Arshad: Writing original draft; Hamdullah Khadim Sheikh, Haroon Khan, Uzma Habib, Faiza Iqbal, and Umbreen Farrukh: Writing review and editing. All authors have read and approved the final manuscript.

Funding

There was no funding.

Data availability statement

The entire dataset of QM calculations performed in this study are available at https://dx.doi.org/10.17632/ypjfdst7nh

Ethical approval

Not applicable.

Conflict of interest

The authors report no competing interests to declare.

Supplementary data

https://www.pjps.pk/uploads/2025/11/SUP1762072761.pdf

REFERENCES

- Benov L (2021). Improved formazan dissolution for bacterial MTT assay. *Microbiol. Spectr.*, **9**(3): e01637-21.
- Cao Y, Qian RC, Li DW and Long YT (2015). Raman/fluorescence dual-sensing and imaging of intracellular pH distribution. *Chem. Commun.*, **51**(99): 17584-17587.
- Ghasemi M, Turnbull T, Sebastian S and Kempson I (2021). The MTT Assay: Utility, Limitations, Pitfalls, and Interpretation in Bulk and Single-Cell Analysis. *Int. J. Mol. Sci.*, **22**(23): 12827.

- Huang H, Huang F, Liang X, Fu Y, Cheng Z, Huang Y, Chen Z, Duan Y and Chen Y (2023). Afatinib reverses EMT via inhibiting CD44-Stat3 axis to promote radio sensitivity in nasopharyngeal carcinoma. *Pharmaceuticals*, **16**(1): 37.
- Hulikova A, Harris AL, Vaughan-Jones RD and Swietach P (2013). Regulation of intracellular pH in cancer cell lines under normoxia and hypoxia. *J. Cell Physiol.*, **228**(4): 743-752.
- Karati D, Mahadik KR, Trivedi P and Kumar D (2022). Alkylating agents, the road less traversed, changing anticancer therapy. *Anti-Cancer Agents Med. Chem.*, **22**(8): 1478-1495.
- Loipersberger M, Bertels LW, Lee J and Head-Gordon M (2021). Exploring the limits of second- and third-order Møller–Plesset perturbation theories for noncovalent interactions: Revisiting MP2.5 and assessing the importance of regularization and reference orbitals. *J. Chem. Theory Comput.*, **17**(9): 5582-5599.
- Malyshkina MV and Novikov AS (2021). Modern software for computer modeling in quantum chemistry and molecular dynamics. *Compounds*, **1**(3): 134-144.
- Paulraj EI and Muthu S (2013). Spectroscopic studies (FTIR, FT-Raman and UV), potential energy surface scan, normal coordinate analysis and NBO analysis of (2R,3R,4R,5S)-1-(2-hydroxyethyl)-2-(hydroxymethyl) piperidine-3,4,5-triol by DFT methods. *Spectrochim. Acta A Mol. Biomol. Spectrosc.*, **108**: 38-49.
- Sheikh HK, Arshad T and Kanwal G (2018). Aryl sulfonate based anticancer alkylating agents. *Pak. J. Pharm. Sci.*, **31**(3): 1081-1085.
- Sheikh, HK, Arshad T, Habib U, Sher Mohammad Z, Ahmed M and Hasan M (2022). Colorimetric chromophoric rapid detection of SARS-CoV-2 through breath analysis. *Pak. J. Pharm. Sci.*, **35**(1): 157-160.
- Sheikh HK, Ortiz CJC, Arshad T, Padrón JM and Khan H (2024). Advancements in steroidal Pt(II) and Pt(IV) derivatives for targeted chemotherapy (2000-2023). *Eur. J. Med. Chem.*, **271**: 116438.